IIETA International Information and Engineering Technology Association
Advancing the World of Information and Engineering

Journal Européen des Systèmes Automatisés
Vol. 59, No. 7, July, 2026, pp. 1995-2006
Journal homepage: http://iieta.org/journals/jesa

An Adaptive Multi-Stage Framework for Underwater Image Enhancement Utilizing Fuzzy Logic Fusion and Perceptual Refinement

Mirza Yogy Kurniawan[1,2*], Pulung Nurtantio Andono[1], Guruh Fajar Shidik[1], Ahmad Zainul Fanani[1]

[1] Faculty of Computer Science, Universitas Dian Nuswantoro, Semarang 50131, Indonesia
[2] Faculty of Information Technology, Universitas Islam Kalimantan Muhammad Arsyad Al Banjari, Banjarmasin 70114, Indonesia

Corresponding Author Email: p41202300069@mhs.dinus.ac.id

https://doi.org/10.18280/jesa.590715

Received: 13 May 2026
Revised: 11 July 2026
Accepted: 23 July 2026
Available online: 31 July 2026

Keywords:
underwater image enhancement, color correction, fuzzy logic fusion, perceptual refinement, Blind/no-Reference Image Spatial Quality Evaluator, Perception-based Image Quality Evaluator, Underwater Color Image Quality Evaluation

ABSTRACT

Underwater images suffer from severe quality degradation, such as non-uniform color distortions, low contrast, and blurred details, caused by wavelength-dependent light absorption and scattering. These coupled distortions severely impair downstream intelligent computer vision tasks, including target detection, keypoint matching, and marine robotic navigation. Conventional underwater image enhancement methods often lack adaptability, as rigid thresholds or single-prior algorithms fail to generalize across diverse water environments. To address these limitations, this study proposes a robust, unsupervised multi-stage pipeline utilizing fuzzy adaptive fusion and sequential refinement. In the first stage, a fuzzy logic-based weighting system analyzes chromaticity in the Commission on Illumination (CIELab) color space to calculate continuous membership weights for blue, green, and yellow casts. These weights execute a soft-switching fusion of three parallel restoration branches: red channel compensation, adaptive white balance, and Gray-world constancy. The second stage applies global Lab white balancing to neutralize residual color shifts. The final stage restores visual clarity by applying contrast-limited adaptive histogram equalization (CLAHE) to the luminance channel and boosting saturation in the Hue, Saturation, Value (HSV) space. Experimental results demonstrate that the proposed method consistently performs well against the existing algorithms. It achieves the highest Underwater Color Image Quality Evaluation (UCIQE) and underwater image quality metric (UIQM) scores, the lowest Perception-based Image Quality Evaluator (PIQE) score, and a highly competitive Blind/no-Reference Image Spatial Quality Evaluator (BRISQUE) score, delivering strong perceptual naturalness, structural sharpness, and balanced color fidelity for underwater images.

1. INTRODUCTION

Underwater image enhancement plays a pivotal role in ocean exploration, marine resource management, and environmental monitoring [1], enabling applications such as underwater robotics [2], marine biology studies, and subsea infrastructure inspection [3]. However, images captured in aquatic environments often suffer from severe degradation due to the selective absorption and scattering of light by water particles [4]. This typically manifests as bluish or greenish casts, along with reduced contrast, blurred details, and limited visibility. These challenges not only hinder visual perception but also impair downstream tasks like object detection, tracking, and segmentation in ocean engineering systems. As the demand for high-quality underwater imagery grows with advancements in autonomous underwater vehicles (AUVs) and remotely operated vehicles (ROVs) [5], effective enhancement techniques are essential to restore natural colors, enhance clarity, and improve overall image usability.

Existing underwater image enhancement methods can be broadly categorized into model-based restoration, vision-based enhancement, and deep learning approaches [6]. Model-based techniques, such as those relying on the dark channel prior (DCP) or polarization imaging, invert the physical degradation process to recover scene properties [7]. Vision-based methods, which include histogram equalization variants like contrast-limited adaptive histogram equalization (CLAHE) [8] and fusion strategies, manipulate pixel values directly for improved contrast and color balance without explicit physics modeling. Recent deep learning advancements, particularly generative adversarial networks (GANs) [9] and transformers [10], have shown superior performance by learning from large datasets.

Beyond GAN- and transformer-based approaches, several additional deep-learning paradigms have recently emerged for underwater image enhancement. Diffusion-based methods, which iteratively refine a noisy image toward a clean target, have been applied to achieve highly detailed and photorealistic restorations; for example, Ding et al. [11] proposed an adversarial-learning-guided diffusion framework, while Shi and Wang [12] introduced a content-preserving conditional diffusion model that explicitly conditions on the raw image at each denoising step to reduce structural drift during generation. Self-supervised approaches, which avoid the need for large paired ground-truth datasets by exploiting cross-view or cross-frame consistency, have also shown promise; Varghese et al. [13] demonstrated joint self-supervised depth recovery and image restoration directly from monocular underwater video, without requiring any reference images. Transformer-based architectures, which model long-range spatial dependencies through self-attention, have likewise advanced the field: Peng et al. [14] proposed a U-shape transformer trained on a large-scale paired dataset with a channel- and spatial-wise attention mechanism specifically designed to address the non-uniform attenuation problem central to underwater imaging.

These deep-learning-based paradigms offer genuine advantages over classical hand-crafted pipelines: they learn highly non-linear, scene-adaptive mappings directly from data, often achieve stronger perceptual realism and structural fidelity on in-distribution test sets, and, in the case of diffusion models, can generate multiple plausible enhancement outcomes rather than a single deterministic result. Recent surveys confirm this trend toward increasingly capable data-driven pipelines [15]. At the same time, as noted above, these advantages are typically accompanied by substantial training-data requirements, high computational and memory costs, and, for diffusion models in particular, iterative sampling procedures that are considerably slower at inference time than single-pass hand-crafted pipelines such as the one proposed in this work. This trade-off motivates the scope of the present study, which targets the complementary niche of a lightweight, training-free alternative rather than competing directly with these data-driven methods on raw perceptual quality.

Despite these advancements, significant gaps persist in current underwater image enhancement techniques, particularly in addressing non-uniform color distortions prevalent in real-world underwater scenes. In this paper, we introduce a robust multi-stage underwater image enhancement pipeline that effectively corrects color distortion and improves visual clarity using fuzzy adaptive fusion and sequential refinement techniques. Initially, we utilize a fuzzy logic-based weighting system for the adaptive classification of underwater color casts. We then implement a parallel enhancement strategy that combines red channel compensation, simple white balance, and gray-world white balance, followed by soft-switching fusion. Furthermore, for refinement stage, we integrate Lab-based white balance as a refinement stage to achieve more neutral and natural color correction and apply visual clarity restoration through enhanced CLAHE and saturation boosting to improve contrast and detail visibility in the final enhanced image.

The scope of this study is explicitly focused on the domain of classical, unsupervised, and non-deep-learning underwater image enhancement methodologies. While recent data-driven networks such as transformers and diffusion models have emerged, they introduce massive computational footprints and heavy training overhead. In contrast, this work aims to pioneer a highly efficient, zero-parameter alternative that pushes the performance boundaries of traditional computer vision techniques. The proposed pipeline relies exclusively on lightweight, CPU-only operations (no GPU acceleration required) without any learned parameters or training data, suggesting promising potential for resource-constrained deployment scenarios such as embedded marine engineering applications. A dedicated per-image runtime and CPU-utilization evaluation supporting this application claim is presented in Section 4.

This paper is organized as follows: Section 1 introduces the challenges of underwater image enhancement. Section 2 reviews the relevant literature on underwater image enhancement, including fuzzy judgment and enhancement stages. Section 3 presents the proposed methodology in detail, including the fuzzy architecture, datasets, and experimental settings. Section 4 discusses the experimental results along with a thorough statistical analysis. Finally, Section 5 concludes the paper and outlines directions for future research.

2. RELATED WORKS

A wide range of enhancement techniques have been developed to mitigate underwater degradations, which are generally classified into four primary categories: Physical Model-Based Restoration, Hybrid Spatial-Domain Compensation, Statistical and Wavelet Fusion Methods, and Deep Learning-Based Approaches. While these methods have advanced the field, each conventional technique possesses distinct architectural drawbacks that limit its generalizability in complex aquatic environments.

Physical Model-Based Restoration: Physical restoration techniques, such as Image Blurriness and Light Absorption (IBLA) proposed by the study [16], invert the Image Formation Model (IFM) by estimating scene depth via IBLA. Similarly, the Underwater Light Attenuation Prior (ULAP) framework [17] utilizes a rapid scene depth estimation prior to recover true scene radiance. However, a major drawback of these methods is their rigid reliance on simplified physical assumptions. For instance, IBLA assumes fixed attenuation coefficients optimized primarily for clear Ocean Type-I water. When applied to highly turbid, real-world coastal or inland waters, these priors fail completely, leading to severe under-restoration or unnatural over-enhancement. Furthermore, these methods evaluate scene parameters globally, making them incapable of handling non-uniform, mixed color casts.

Hybrid Spatial-Domain Compensation: To minimize reliance on strict physical priors, spatial domain methods utilize localized transformations. Zhang et al. [18] implemented adaptive color correction by dividing color distortions into deterministic cases, while Li et al. [19] used a rigid Heaviside function to partition image channels into subsets. The primary drawback of these techniques lies in their hard-thresholding or discrete classification approach. By forcing an image into a rigid color-tone category (e.g., purely green or purely blue), these algorithms create unnatural boundary artifacts and severe color distortion when encountering ambiguous or hybrid color casts (e.g., mixed blue-green water profiles). Minimal Color Loss and Locally Adaptive Contrast Enhancement (MLLE) by the study [20] operates entirely within the spatial domain, prioritizing the minimization oppresses global color over-saturation by penalizing deviations from the original color ratios; its structural drawback stems from its purely localized mapping functions. Without a global color-cast judgment engine, it tends to preserve or even amplify fine-grained, non-uniform background color casts, which degrades its performance under highly turbid water conditions.

Statistical and Wavelet Fusion Methods: Advanced vision-based methods employ multi-scale or frequency-domain fusion strategies. Wang et al. [21] introduced normalization ranges based on channel similarity, while Shi et al. [22] utilized piecewise color correction, and Zhang et al. [23] incorporated wavelet decomposition fusion of advantage contrast (WFAC). Although effective at boosting local contrast, these methods exhibit a critical drawback: they lack an integrated global stabilization mechanism. Consequently, aggressively boosting contrast and saturation layer-by-layer accumulates residual global color biases, frequently generating over-saturated images with elevated perceptual distortion. WFAC [23] shifts the enhancement pipeline into the frequency domain by employing discrete wavelet transform (DWT) to decompose the degraded image into high-frequency (detail) and low-frequency (approximation) sub-bands. It extracts spatial gradient distributions and optimizes the integration statistics layer-by-layer to fuse advanced contrast attributes. However, the fundamental limitation of WFAC lies in its frequency-decoupled optimization strategy. Because it sharpens edge gradients aggressively in the high-frequency sub-bands before inverse DWT, it lacks an integrated global stabilization layer to regulate the chromaticity vectors. Advantage Feature Weighted Fusion (AFWF) [24] is a multi-scale hybrid framework that segregates contrast and color attributes into distinct structural components. It calculates pixel-level advantage feature maps and selectively merges them using a deterministic layer-by-layer weighted fusion strategy. Although AFWF achieves high colorfulness metrics by aggressively amplifying specific attenuated bands, its primary architectural flaw is its hard-decision fusion logic.

Deep Learning-Based Approaches: Data-driven architectures like GANs [9], MD-Net [25], and CAFS-Net [26] learn direct mapping functions from large paired datasets. The critical drawbacks here are massive computational overhead, substantial parameter footprints, and heavy dependency on synthetic training data. These factors make them highly unsuitable for real-time deployment on hardware-constrained embedded processors embedded within AUVs and ROVs.

The critical research gap in current underwater image enhancement literature is the lack of a lightweight, unsupervised mechanism that can adaptively balance color channels under mixed and ambiguous color casts without relying on rigid, discrete thresholds. Conventional methods either over-simplify the environment via rigid physical priors or introduce artificial boundary texturing through hard case-switching logic.

3. PROPOSED METHODOLOGY

This paper proposes an unsupervised underwater image enhancement framework that effectively restores color fidelity, improves contrast, and enhances perceptual quality without relying on deep learning or paired training data. The method is designed to overcome the limitations of rigid classification approaches by introducing a fuzzy-logic-based soft-switching mechanism that dynamically adapts to mixed or ambiguous color casts commonly found in real-world underwater scenes. By integrating adaptive color correction, global white balance in Lab space, and a final perceptual refinement stage, the proposed pipeline achieves robust performance across varying turbidity levels while maintaining computational efficiency that is well-suited for lightweight, low-resource deployment scenarios in ocean engineering.

Unlike conventional methods, our approach utilizes fuzzy membership weights derived from mean chromaticity in Lab space. This soft decision-making strategy allows each pixel to be corrected by a weighted combination of specialized algorithms tailored for bluish, greenish, and yellowish casts. Such a mechanism significantly reduces over-correction artifacts and improves generalization, particularly in images containing hybrid color distortions or non-uniform lighting conditions.

The overall pipeline consists of three sequential stages. First, a fuzzy-weighted adaptive color correction module performs soft fusion of three complementary correction strategies. Second, a global Lab white-balance step further neutralizes residual color biases. Finally, a perceptual enhancement module simultaneously boosts contrast through CLAHE and increases colorfulness via saturation adjustment in HSV space. The complete framework is illustrated in Figure 1. The following subsections detail each stage of the proposed method.

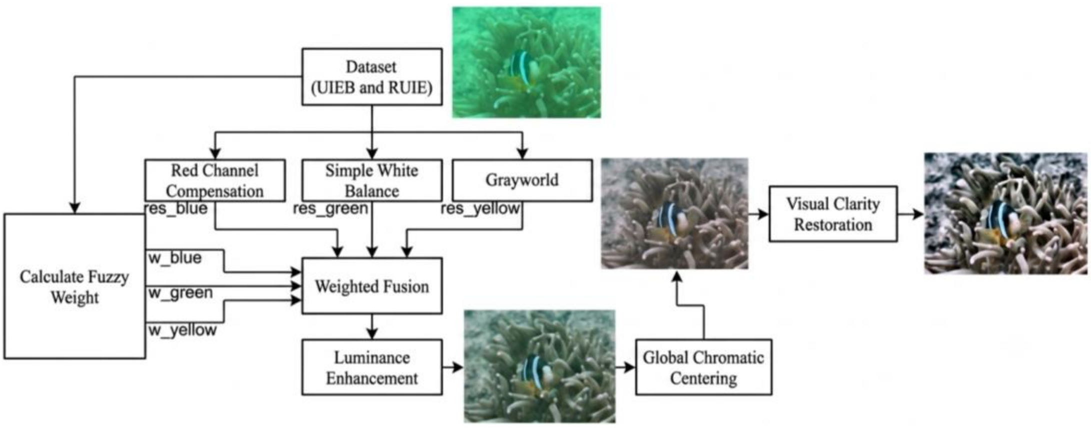

Figure 1. Proposed architecture of fuzzy weighted adaptive color correction

3.1 Fuzzy-weighted adaptive color correction

We first load the input image and convert it to the Lab color space for analysis, as chromaticity (a, b channels) and luminance (L channel) are decoupled. To determine the degree of color cast, we compute fuzzy membership weights based on the mean chromaticity of the a and b channels.

The mean chromaticity is calculated as:

$$m_a = \frac{1}{H \times W} \sum_{i=1}^{H} \sum_{j=1}^{W} (a(i,j)) - 128 \quad (1)$$

$$m_b = \frac{1}{H \times W} \sum_{i=1}^{H} \sum_{j=1}^{W} (b(i,j)) - 128 \quad (2)$$

where, H and W are image height and width, and normalization shifts to [-128, 127] range. Fuzzy weights for blue (w_blue), green (w_green), and yellow (w_yellow) casts are then derived:

$$w_{blue} = ma\,x(0 - m_b)\,/(|m_a| + |m_b| + \epsilon) \quad (3)$$

$$w_{green} = ma\,x(0 - m_a)\,/(|m_a| + |m_b| + \epsilon) \quad (4)$$

$$w_{yellow} = max\left(0{,}1 - \left(w_{blue} + w_{green}\right)\right) \quad (5)$$

with $\varepsilon = 10^{-6}$ to avoid division by zero. This soft assignment allows gradual transitions for images with hybrid casts, reducing artifacts in boundary cases.

Algorithm 1. Fuzzy-Weighted Adaptive Color Correction (Stage 1)

Input: RGB underwater image I
Output: Color-corrected image I_corr

1. Convert I from RGB to Lab color space → obtain L, a, b channels
2. Compute mean chromaticity deviations:
    m_a ← (1/(H×W)) · Σ_i Σ_j (a(i,j) − 128) (Eq. (1))
    m_b ← (1/(H×W)) · Σ_i Σ_j (b(i,j) − 128) (Eq. (2))
3. Compute fuzzy membership weights:
    w_blue ← max (0, −m_b) / (|m_a| + |m_b| + ε) (Eq. (3))
    w_green ← max (0, −m_a) / (|m_a| + |m_b| + ε) (Eq. (4))
    w_yellow ← max (0, 1 − (w_blue + w_green)) (Eq. (5))
    # w_blue + w_green + w_yellow = 1 (partition of unity)
    # ε = 1e-6 (fixed numerical-stability constant)
4. Apply the three specialized correction branches to I:
    I_red ← Red-Channel Compensation(I) (Eq. (6))
    I_lab ← LabShiftWhite Balance(I) (Eqs. (7)-(8))
    I_gray ← Gray-worldWhite Balance(I)
5. Fuse branches using the fuzzy weights (soft-switching fusion):
    I_corr ← w_blue·I_red + w_green·I_lab + w_yellow·I_gray
6. Clip I_corr to valid range [0, 255]
Return I_corr

In the CIE Lab color space, a channel encodes the green–red chromatic axis (negative values indicating a green shift, positive values indicating a red shift), while the b channel encodes the blue–yellow chromatic axis (negative values indicating a blue shift, positive values indicating a yellow shift). The proposed membership weights are derived directly from this geometric property: w_blue captures the magnitude of the negative deviation of m_b (Eq. (3)), w_green captures the magnitude of the negative deviation of m_a (Eq. (4)), and w_yellow is obtained as the complementary residual (Eq. (5)), representing the remaining positive-b tendency not already accounted for by the blue and green components.

Both w_blue and w_green are normalized by the total absolute chromatic deviation, |m_a| + |m_b| + ε, which bounds each weight to the range [0, 1]. Since w_yellow is defined as max(0, 1 − (w_blue + w_green)), the three weights always satisfy w_blue + w_green + w_yellow = 1, forming a valid convex combination (partition of unity) regardless of the input image's chromatic content. The term $\varepsilon = 10^{-6}$ is a fixed numerical-stability constant used solely to prevent division by zero when m_a = m_b = 0 (i.e., a perfectly neutral image); it is not an environment-dependent parameter and requires no manual tuning across different underwater scenes, consistent with the unsupervised, zero-parameter design goal of the proposed framework. Algorithm 1 summarizes the complete procedure for computing and applying the fuzzy fusion weights, allowing full reproducibility of this stage.

The choice of blue, green, and yellow as the three primary correction categories follows directly from the geometry of the CIE Lab chromaticity plane rather than being an arbitrary design choice. The two chromaticity axes (a: green–red, b: blue–yellow) naturally span four quadrant directions; however, in underwater imagery the red-shift direction of the a-axis is rarely observed as a dominant cast, since red wavelengths are attenuated first and most severely by water, leaving the green-shift direction as the practically relevant pole of that axis. Combined with the two poles of the b-axis (blue and yellow), this yields the three dominant, empirically observed cast categories addressed by the proposed framework, which is consistent with the color distributions reported for the Underwater Image Enhancement Benchmark (UIEB) and Underwater Color Cast Set (UCCS) benchmark datasets used in this study. We acknowledge that other underwater conditions, such as cyan-dominant casts, mixed artificial-natural illumination, or severe low-light scenes, are not explicitly modeled as separate categories; these fall outside the primary scope of the proposed fuzzy weighting scheme and are discussed as a limitation in Section 5.

Based on these weights, we apply three specialized correction algorithms and fuse them softly:

For dominant blue casts (high w_blue) we use red channel compensation to a local adaptive form:

$$r_{comp}(x,y) = r(x,y) + (\overline{g} - \overline{r}) \cdot g(x,y) \cdot \left(1 - r(x,y)\right) \quad (6)$$

where, r, g, and b are normalized channels (0-1), and overlines denote means. This avoids purple artifacts by emphasizing green-red balance.

For dominant green casts (high w_green), we use simple white balance in Lab, shifting a and b toward neutral:

$$\acute{a} = a - \left((\overline{a} - 128) \cdot (L/255) \cdot 1.1\right) \quad (7)$$

$$\acute{b} = b - \left((\overline{b} - 128) \cdot (L/255) \cdot 1.1\right) \quad (8)$$

For dominant yellow casts (high w_yellow), we use gray-world white balance, assuming average scene reflectance is achromatic.

3.2 Lab white balance

To further refine color neutrality, we apply a global white balance in Lab space on the output of the previous stage. This step corrects residual biases by centering a and b means at 128:

$$\acute{a} = a - (\overline{a} - 128) \tag{9}$$

$$\acute{b} = b - (\overline{b} - 128) \tag{10}$$

Clipping ensures [0, 255] range. This complements the fuzzy correction, addressing global shifts missed in local adaptations, and improves upon channel-specific compensation by leveraging Lab's perceptual uniformity.

3.3 Visual clarity restoration

The final stage, termed visual clarity restoration, is applied to further enhance perceptual quality after fuzzy-weighted color correction and global Lab white balance. First, a gray-world white balance is performed to neutralize residual color cast by assuming the average color of the scene is gray. The image is then converted to Lab color space, where CLAHE with clipLimit = 3.0 and tileGridSize = (8,8) is applied exclusively to the luminance channel (L) to improve local contrast while avoiding over-enhancement and blocking artifacts. Subsequently, the image is transformed to HSV color space, and the saturation channel is boosted by a factor of 1.5 (with clipping to maintain the valid range) to increase color vividness and chroma without altering hue or value. Finally, the image is converted back to the BGR color space. This module specifically targets the three key components of underwater image quality: contrast, saturation, and colorfulness, thereby significantly improving visual clarity and perceptual appeal in real-world underwater scenes.

4. RESULTS AND DISCUSSION

The effectiveness of the proposed method from this study for color improvement and enhancement, we conducted a series of experiments using publicly available image datasets: the UIEB [27] and the UCCS [28]. UIEB contains 950 data points consisting of 890 paired raw and reference data and 60 challenging data. In this study, only 890 raw datasets were used. The UCCS dataset, which is part of the RUIE dataset, has three subsets, namely blue, blue-green, and green, where each subset consists of 100 underwater images.

All 890 raw images from the UIEB dataset and all 300 images from the UCCS dataset (100 from each of its three subsets: blue, blue-green, and green) were evaluated in every experiment reported in this study, with no additional sampling, filtering, or exclusion applied. Each image was processed at its original size and resolution as provided in the source dataset; no resizing, cropping, or other preprocessing step was applied prior to enhancement, so that the reported results directly reflect the pipeline's behavior on unmodified, real-world underwater images of varying dimensions. Because the proposed pipeline is a fully deterministic image-processing framework, containing no learned parameters, random initialization, or stochastic components, repeated execution on the same input image under identical settings produces bit-identical output images and therefore identical quality-metric scores. The experiments were executed multiple times to confirm this deterministic behavior; since no run-to-run variance was observed, a single recorded run is reported for each dataset in Section 4.1.

Due to the absence of ground-truth references for real-world underwater scenes, no-reference metrics are used for objective image quality assessment. This research adopts four image quality evaluation metrics, namely Blind/no-Reference Image Spatial Quality Evaluator (BRISQUE) [29], Perception-based Image Quality Evaluator (PIQE) [30], Underwater Color Image Quality Evaluation (UCIQE) [31], underwater image quality metric (UIQM) [32]. Image quality measured by UCIQE quantifies the quality of underwater images by using a linear weighted combination of chromaticity, saturation, and contrast, thereby evaluating the effects of blurring, non-uniform color cast, and low contrast of underwater images. UCIQE scores are positively correlated with image quality: the larger the value, the better the quality.

$$UCIQE = c_1 \times \sigma_c + c_2 \times con_l + c_3 \times \mu_s \tag{11}$$

where, c_1, c_2 and c_3 are the coefficient factors (c_1 = 0.4680, c_2 = 0.2745, and c_3 = 0.2576), σ_c is the standard deviation of chroma; con_l is the contrast of brightness, and μ_s is the average of saturation as the original paper [31]. UIQM is made up of three underwater image attribute measures, specifically the Underwater Image Colorfulness Measure (UICM), the Underwater Image Sharpness Measure (UISM), and the Underwater Image Contrast Measure (UIConM). UIQM is formulated as a linear combination expressed as follows:

$$UIQM = c_1 \times UICM + c_2 \times UISM + c_3 \times UIConM \tag{12}$$

where, c_1, c_2 and c_3 are scaling coefficients. These are set to c_1 = 0.0282, c_2 = 0.2953, and c_3 = 3.5753 as proposed in the original paper [32]. BRISQUE is a no-reference quality metric designed to measure the naturalness of images by analyzing statistical deviations from a model of natural scene statistics, yielding scores from 0 to 100. The smaller the deviation and hence the lower the BRISQUE value, the more natural the image appears. To summarize, a larger UIQM value signifies richer colors, sharper edges, and higher contrast in underwater images, whereas a smaller BRISQUE value implies a more natural and realistic image quality [29]. PIQE is a no-reference image quality assessment metric whose score is inversely proportional to the actual image quality. The smaller the PIQE score, the higher the perceived quality of the image.

The proposed method employs a multi-stage pipeline to adaptively rectify colour distortions and improve perceptual quality for each input image. Initially, three concurrent colour compensation branches are implemented: red channel compensation to rectify red-channel attenuation in underwater images, simple white balance to standardise global illumination, and gray-world assumption to assess and correct colour casts throughout the scene. The outputs from these three branches are subsequently input into a fuzzy weight calculation module, which determines adaptive fusion weights (w_blue, w_green, w_yellow) according to the predominant colour distribution of the input image. The weights regulate the Weighted Fusion stage, wherein the three adjusted outputs are subtly combined in accordance with the identified colour

cast, a core soft-switching characteristic that differentiates the proposed method from hard-decision fusion strategies. The amalgamated result is then subjected to visual clarity restoration to retrieve intricate structural details, succeeded by Luminance Enhancement and Global Chromatic Centring to achieve the final perceptual equilibrium of the output image.
To ensure a fair, rigorous, and reproducible comparative evaluation, the proposed multi-stage framework and all five non-deep-learning baseline methodologies IBLA [16], ULAP [17], MLLE [20], WFAC [23], and AFWF [24]. These methods were executed and benchmarked from scratch under an identical computational environment. The proposed pipeline is implemented using the Python programming language version 3.13.7, utilizing core digital image processing libraries, specifically OpenCV and NumPy. All experiments, statistical computations, and runtime evaluations were carried out on a standardized local workstation equipped with an Intel Core i5-12400F CPU and 32 GB of RAM, running in a CPU-only execution mode (no GPU acceleration) to evaluate the native algorithmic efficiency.

To evaluate the quantitative and qualitative efficacy of the proposed framework, extensive comparisons are conducted strictly against representative and state-of-the-art non-deep-learning baselines. To maintain a fair and scientifically consistent architectural evaluation, our method is not benchmarked against learning-based transformer or diffusion paradigms. Instead, the comparative scope is deliberately focused on classical and advanced hand-crafted frameworks, verifying that our fuzzy soft-switching engine achieves superior optimization within the unsupervised domain.

4.1 Results on the UIEB dataset

The results obtained from the evaluation on the UIEB dataset are presented in Figure 2.

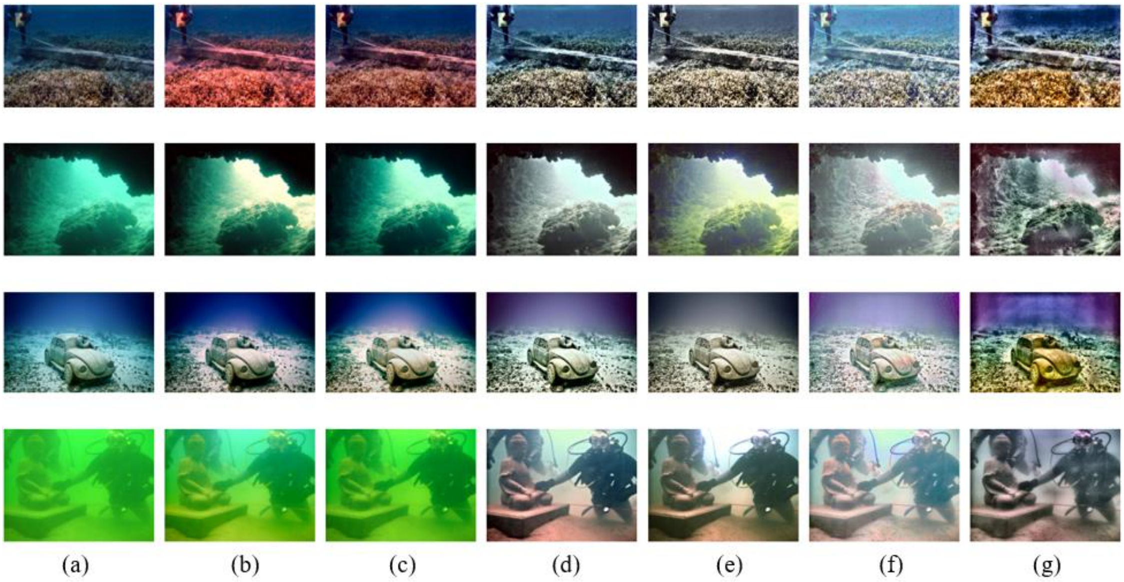

Figure 2. Visual comparison on the Underwater Image Enhancement Benchmark (UIEB) dataset from left to right: (a) raw, (b) Image Blurriness and Light Absorption (IBLA), (c) Underwater Light Attenuation Prior (ULAP), (d) MLLE, (e) WFAC, (f) AFWF, and (g) our method

Table 1. Average quantitative performance comparison of various methods on the UIEB dataset

Methods	UCIQE↑	UIQM↑	BRISQUE↓	PIQE↓
IBLA	0.596	3.993	30.249	36.247
ULAP	0.603	3.547	28.546	33.162
MLLE	0.606	3.761	26.670	37.287
WFAC	0.611	3.838	25.986	32.801
AFWF	0.534	4.228	27.624	35.128
Ours	0.632	4.654	26.090	30.780

Note: Underwater Image Enhancement Benchmark (UIEB); Image Blurriness and Light Absorption (IBLA); Underwater Light Attenuation Prior (ULAP); Underwater Color Image Quality Evaluation (UCIQE); underwater image quality metric (UIQM); Blind/no-Reference Image Spatial Quality Evaluator (BRISQUE); Perception-based Image Quality Evaluator (PIQE).

As presented in Table 1, the proposed multi-stage pipeline achieves the highest scores among the compared methods in both underwater-specific quality criteria (UCIQE and UIQM), while also obtaining the lowest (best) PIQE score and a competitive BRISQUE score. Specifically, our method achieves a peak UCIQE score of 0.632 and a leading UIQM score of 4.654, outperforming the second-best methods by significant margins. A rigorous analysis of the underlying metric formulations explains this superior behavior. Traditional spatial domain techniques like MLLE [15] and multi-scale fusion methods like AFWF [19] frequently suffer from a severe decoupling penalty: aggressively boosting chromatic saturation to optimize UCIQE or sharpening high-frequency components to elevate UIQM usually induces severe over-saturation, color artifacts, and localized distortion.

This fundamental conflict is clearly visible in the baseline data; for instance, while AFWF achieves a high UIQM of 4.228, its rigid case-switching boundaries yield a degraded UCIQE of 0.534 and an elevated PIQE of 35.128 due to artificial edge distortions.

Consequently, the localized texture details and edges are recovered harmoniously, as mathematically validated by our lowest (best) PIQE score of 30.780, which outpaces the second-best method (WFAC) by a substantial margin of 2.021 points. The quantitative outcomes on the UIEB dataset demonstrate that the proposed fuzzy adaptive framework successfully establishes an optimal equilibrium between aggressive color-contrast restoration and natural aesthetic preservation.

Figure 3 illustrates the comparative visual results of various methods on the UIEB dataset.

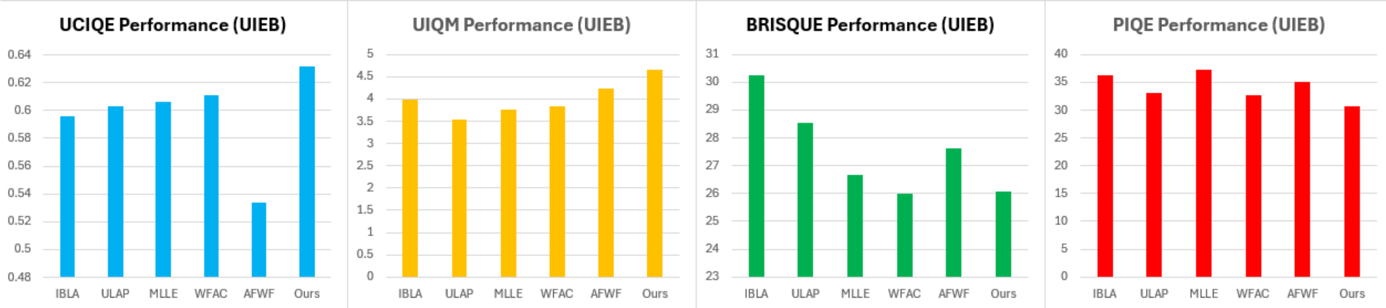

Figure 3. Quantitative evaluation of the ablation study on the Underwater Image Enhancement Benchmark (UIEB) dataset

4.2 Results on the Underwater Color Cast Set dataset

To further verify the generalization capability and robustness of the proposed framework across distinct real-world underwater color tones, extensive quantitative evaluations were carried out on the UCCS dataset. The UCCS benchmark incorporates diverse underwater subsets heavily degraded by localized bluish, greenish, and blue-greenish color casts. The average quantitative performance comparison between the proposed method and the five baseline algorithms is comprehensive and documented in Table 2.

Table 2. Average quantitative performance comparison of various methods on the Underwater Color Cast Set (UCCS) dataset

Methods	UCIQE↑	UIQM↑	BRISQUE↓	PIQE↓
IBLA	0.480	1.289	31.964	36.742
ULAP	0.465	1.630	31.744	36.722
MLLE	0.574	4.068	25.110	32.830
WFAC	0.602	4.120	28.420	31.785
AFWF	0.491	4.516	29.644	28.800
Ours	0.543	4.846	25.044	21.582

The experimental data summarized in Table 2 reveal that the proposed framework delivers an outstanding performance, securing the best scores in three out of the four evaluation metrics. Most notably, our method achieves a peak UIQM score of 4.846, while simultaneously yielding the lowest spatial distortion metrics with a BRISQUE score of 25.044 and a PIQE score of 21.582. Compared to the second-best methods in each category, our model improves the UIQM by 0.330 points (against AFWF) and pushes the PIQE down by a substantial margin of 7.218 points against AFWF.

From a theoretical perspective, the consistent dominance of our method across the UIQM, BRISQUE, and PIQE metrics validates the mathematical core of the fuzzy logic soft-switching fusion layer. The UCCS dataset presents a significant challenge due to its highly fluid, non- uniform distributions of light scattering. Conventional baseline frameworks, such as MLLE and AFWF, process images using deterministic or rigid thresholding category boundaries. When an image contains an overlapping color cast (e.g., green-blue turbidity), these hard boundaries force a localized step-function behavior during channel amplification. This mathematical discontinuity introduces severe structural artifacts and block-level noise, which manifests directly as inflated PIQE and BRISQUE scores. In contrast, our pipeline derives continuous fractional membership weights (w_blue, w_green, w_yellow) from the mean chromaticity components in the CIE Lab color space. This soft assignment allows the parallel restoration pathways to merge smoothly at the pixel level, preventing artificial color transition boundaries and significantly preserving natural scene statistics.

Furthermore, analyzing the UCIQE metric reveals a highly insightful mathematical trade-off that highlights the stability of our architecture. As observed in Table 2, WFAC and MLLE achieve higher raw UCIQE scores (0.602 and 0.574, respectively) compared to our stable score of 0.543. However, a deeper scientific look into the UCIQE mathematical formulation explains this phenomenon. The UCIQE metric is fundamentally driven by the standard deviation of chroma. Algorithms that employ aggressive local contrast stretching or independent channel-by-channel transformations without global stabilization layers can artificially inflate the σc vector by generating severe, unnatural color variances across local windows. While this mathematically maximizes the raw UCIQE score, it damages holistic human perception by inducing over-saturation and ringing artifacts, as evidenced by WFAC's elevated PIQE score of 31.785 and MLLE's BRISQUE score of 25.110. The proposed framework successfully circumvents this optimization penalty through its decoupled multi-stage design. By placing an explicit global Lab white balance (Stage 2) immediately after the fuzzy adaptive fusion and prior to the visual clarity restoration module (Stage 3), the framework ensures color constancy across the scene. Stage 2 effectively centers the a and b distributions to prevent the amplification of dominant color distortions. Subsequently, Stage 3 optimizes luminance contrast through CLAHE and boosts saturation in the HSV space under controlled thresholds. This decoupled arrangement allows our method to maximize edge sharpness and sharpness-driven contrast, explaining the outstanding UIQM score of 4.846 while preventing the explosion of local chromaticity artifacts. The overall quantitative results on the UCCS dataset indicate that the proposed framework generalizes effectively across varying water-color conditions, providing a well-balanced and stable enhancement solution for underwater computer vision tasks, within the scope of the two datasets and four no-reference metrics evaluated in this study. Figure 4 provides a visual comparison of the enhancement results on the UCCS dataset, while Figure 5 demonstrates the performance results obtained from applying the proposed framework to the UCCS dataset.

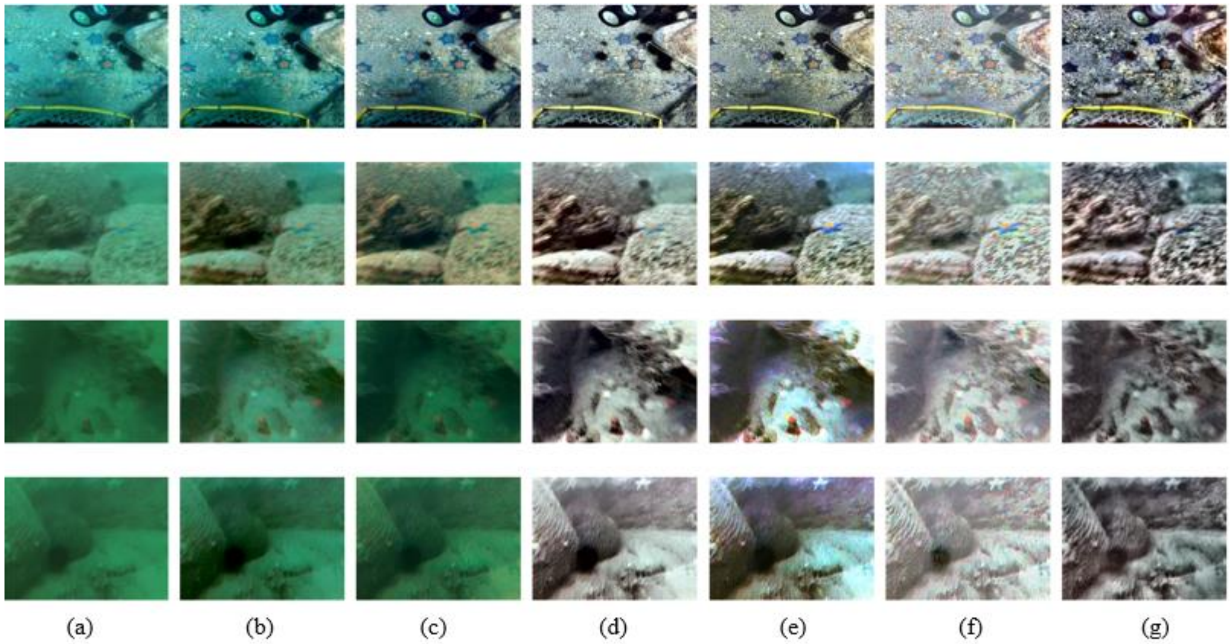

Figure 4. Visual comparison on the Underwater Color Cast Set (UCCS) dataset from left to right: (a) raw, (b) Image Blurriness and Light Absorption (IBLA), (c) Underwater Light Attenuation Prior (ULAP), (d) MLLE, (e) WFAC, (f) AFWF, and (g) our method

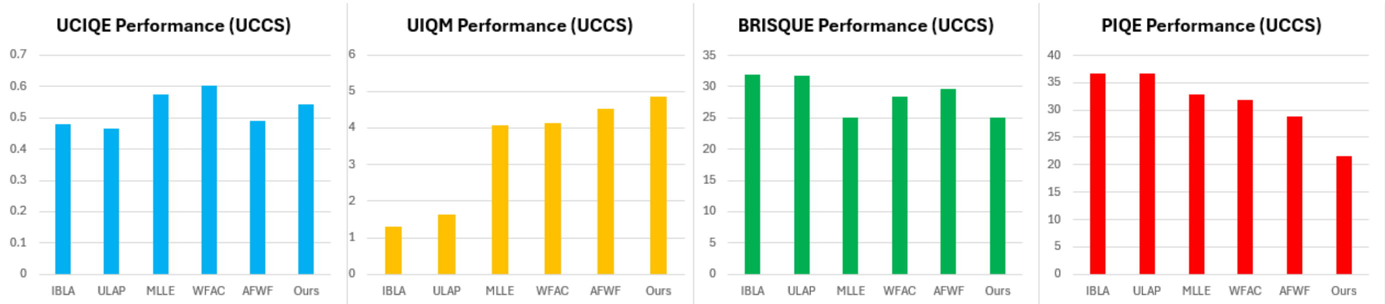

Figure 5. Quantitative evaluation of the ablation study on the Underwater Color Cast Set (UCCS) dataset

4.3 Validation

To validate the individual contributions and empirical necessity of each phase within the proposed multi-stage framework, a comprehensive ablation study was conducted on the UIEB dataset. The proposed pipeline comprises three distinct processing components: the first stage (Fuzzy-weighted Adaptive Fusion), the second stage (Lab White Balance), and the third stage (Visual Clarity Restoration). The performance of each structural variant was quantitatively assessed using four widely accepted non-reference image quality metrics: UCIQE, UIQM, BRISQUE, and PIQE. The quantitative outcomes of this analysis are documented in Table 3.

Table 3. Ablation study on the Underwater Image Enhancement Benchmark (UIEB) dataset

Methods	UCIQE↑	UIQM↑	BRISQUE↓	PIQE↓
-w/o FACC	0.592	4.365	23.473	29.767
-w/o LWB	0.619	4.511	25.952	30.958
-w/o VCR	0.562	4.303	23.975	29.962
Full model	0.632	4.654	26.090	30.780

The removal of the first stage (-w/o FACC), which eliminates the fuzzy logic-driven soft-switching fusion of the parallel specialized restoration pathways, results in a distinct degradation of initial color balancing. This structural omission leads to a lower UCIQE score of 0.592 compared to the full model's score of 0.632. Without the adaptive fuzzy weighting mechanism, the system cannot dynamically adapt to specific color-cast tendencies, thereby highlighting the importance of the fuzzy decision framework in managing diverse water conditions.

When the second stage is omitted (-w/o LWB), the pipeline operates without the global color stabilization layer in the CIE Lab space. This variant produces a slightly lower UCIQE score of 0.619 and a lower UIQM score of 4.511 compared to the full model, indicating that the global stabilization step meaningfully contributes to color balance and structural-perceptual quality on this dataset. Notably, the BRISQUE score is marginally lower (better) without this stage, 25.952 versus 26.090 for the full model. This isolated exception suggests that the second stage's contribution is not uniformly positive across every metric; rather, it primarily targets residual chromatic bias rather than the general spatial-naturalness characteristics captured by BRISQUE. Overall, the second stage still functions as a valuable stabilization layer, though its benefit is best understood as complementary to, rather than strictly necessary for, every individual quality indicator.

Table 4. Ablation study on the Underwater Color Cast Set (UCCS) dataset

Methods	UCIQE↑	UIQM↑	BRISQUE↓	PIQE↓
-w/o FACC	0.487	4.117	25.058	29.302
-w/o LWB	0.533	4.766	25.980	22.059
-w/o VCR	0.448	3.775	26.037	31.795
Full model	0.543	4.846	25.044	21.582

The most substantial performance drop occurs when excluding the third stage (-w/o VCR), which is responsible for CLAHE and adaptive saturation adjustments. Without this visual clarity restoration phase, the UCIQE score drastically plunges to its lowest recorded value of 0.562. Because the third stage directly optimizes luminance contrast, local edge sharpness, and colorfulness components, the primary constituent coefficients of the UCIQE metric, its elimination fundamentally undermines the framework's capability to recover intricate texture details and visibility degraded by underwater light scattering. Ultimately, the Full model achieves the most optimal and well-rounded performance across all evaluation criteria. It balances the specialized restoration vectors to achieve a high UIQM score of 4.654 and a stable UCIQE score of 0.632, while maintaining highly competitive general-purpose natural scene statistic distributions with a BRISQUE score of 26.090 and a PIQE score of 30.780. These ablation results indicate that each stage of the proposed pipeline contributes meaningfully to overall performance, although the magnitude and direction of this contribution vary across individual metrics. The first and third stages consistently improve every evaluated metric on this dataset, whereas the second stage's benefit is concentrated on color-balance-related metrics rather than uniformly improving all four indicators. To verify the structural necessity and individual performance contributions of each constituent phase in the proposed framework, a rigorous ablation study was performed on the UCCS dataset. The performance of the complete model against its stripped-down variants was quantitatively evaluated using four benchmark no-reference image quality metrics: UCIQE, UIQM, BRISQUE, and PIQE. Higher values for UCIQE and UIQM indicate superior color, sharpness, and contrast balance, while lower scores for BRISQUE and PIQE denote reduced distortion and enhanced naturalness. The experimental data is compiled in Table 4.

The exclusion of the first stage (-w/o FACC), which replaces the fuzzy-logic soft-switching fusion framework with a static processing route, yields a notable drop in color restoration capability. Without the adaptive pixel-level weighting derived from the CIE Lab chromaticity statistics, the model's ability to handle diverse underwater color casts diminishes, causing the UCIQE score to decrease to 0.487 and the UIQM score to drop to 4.117. Concurrently, perceptual degradation is evidenced by the inflation of the PIQE score to 29.302, confirming that the fuzzy decision system is essential for guiding the initial parallel restoration pillars effectively.

Omitting the second stage (-w/o LWB) removes the global color stabilization layer executed within the Lab color space. This variant produces an isolated UCIQE score of 0.533, which is slightly closer to the full model. However, this marginal inflation is counterbalanced by an evident degradation across all other metrics: the UIQM score declines to 4.766, the BRISQUE score rises to 25.980, and the PIQE score rises to 22.059. This behavior occurs because the absence of the global stabilization step allows unchecked chromatic shifts or localized over-saturation to persist. While these raw chromatic variations can artificially elevate the standard deviation vectors in the UCIQE formula, they introduce distortion that undermines holistic human perception, a regression accurately captured by the worsening UIQM, BRISQUE, and PIQE scores.

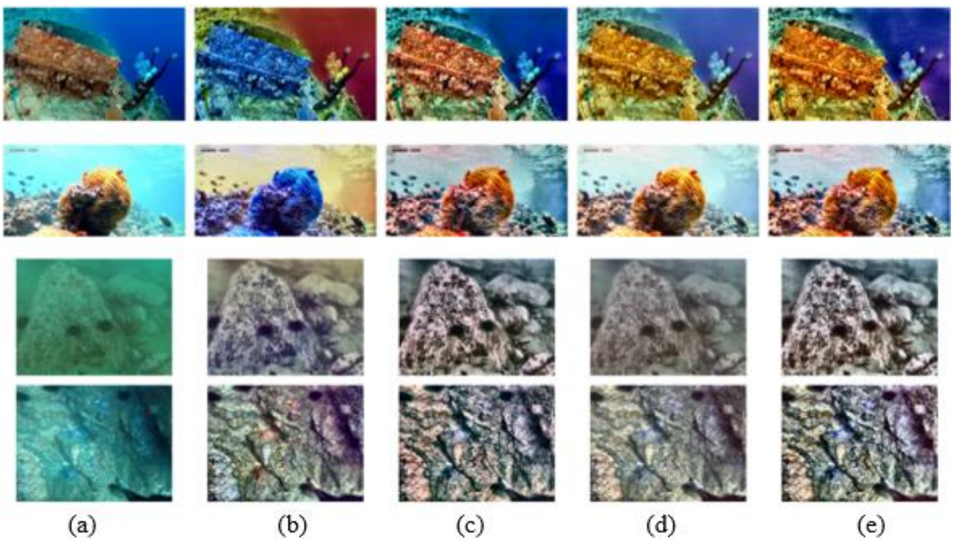

Figure 6. Qualitative visual comparison of each step. From left to right: (a) raw image, (b) without FACC, (c) without LWB, (d) without VCR, and (e) full model

The most severe performance collapse is observed when the third stage is eliminated (-w/o VCR), bypassing the luminance contrast equalization via CLAHE and the adaptive saturation optimization in the HSV space. Without this clarity restoration layer, the framework fails to counteract underwater light scattering and haze, forcing the UCIQE and UIQM scores down to their lowest values of 0.448 and 3.775, respectively. Furthermore, spatial distortion and block-level unnaturalness reach their worst levels, as shown by a BRISQUE score of 26.037 and a PIQE score of 31.794. These results demonstrate that the final stage is critical for recovering structural details and edge sharpness. In contrast, the full model demonstrates the most balanced and superior overall performance. It registers the highest UIQM score (4.846) and achieves the lowest (best) scores for both BRISQUE (25.044) and PIQE (21.582), while stabilizing the UCIQE score at a reliable 0.543. By successfully integrating all three stages, the full model avoids over-saturation and artifacts while maximizing structural clarity and color fidelity. This ablation analysis on the UCCS dataset shows a more consistent pattern than on UIEB: each stage's removal degrades every evaluated metric, supporting a complementary and cooperative role for the three stages under this dataset's more severe and uniform color-cast conditions. Figure 6 shows the qualitative visual comparison of each step. To evaluate the computational efficiency claims made in Section 1, per-image runtime and CPU utilization were measured while processing the complete UIEB (n = 890) and UCCS (n = 300) datasets on the workstation described above. For each image, wall-clock processing time was recorded independently for each of the three pipeline stages using high-resolution timers, and CPU utilization was sampled via the OS process monitor. Table 5 summarizes these results. We note that the reported CPU utilization values commonly exceed 100%, reflecting OpenCV's internal multi-threaded execution across multiple CPU cores; this clarifies that the experimental setup is CPU-only (no GPU acceleration) rather than strictly single-threaded.

Table 5. Per-image runtime and CPU utilization on the Underwater Image Enhancement Benchmark (UIEB) and Underwater Color Cast Set (UCCS) datasets

Dataset	N	Total Time (ms) Mean ± SD	Median (ms)	img/s	CPU Util. (%) Mean ± SD
UIEB	890	90.24 ± 84.02	48.97	11.1	150.98 ± 103.90
UCCS	300	16.28 ± 5.09	15.97	61.4	158.81 ± 176.34

The average total processing time was 90.24 ± 84.02 ms per image on the UIEB dataset (median 48.97 ms; throughput ≈ 11.1 images/second) and 16.28 ± 5.09 ms per image on the UCCS dataset (median 15.97 ms; throughput ≈ 61.4 images/second). This difference reflects the substantial variation in image resolution between the two datasets: UIEB images range from 225 × 159 to 2180 × 1450 pixels (mean 0.63 megapixels), whereas UCCS images are uniformly 400 × 300 pixels (0.12 megapixels), indicating that processing time scales primarily with input resolution rather than with content-dependent factors such as the severity of the color cast. Averaged across both datasets, the fuzzy-weighted adaptive color correction stage (Stage 1) accounts for the majority of total processing time (67.9 ms on UIEB, 11.4 ms on UCCS), followed by the Lab white balance (Stage 2, 12.8/2.6 ms) and visual clarity restoration (Stage 3, 9.5/2.3 ms) stages, both of which contribute a comparatively small and stable overhead across image sizes. These results indicate that the proposed pipeline is computationally lightweight relative to typical deep-learning-based enhancement methods, which commonly require GPU acceleration to achieve comparable throughput; we emphasize, however, that a direct runtime comparison against such baselines, as well as evaluation on actual embedded hardware (e.g., an AUV/ROV onboard computer), is left for future work.

5. CONCLUSIONS

This paper has presented a robust and highly adaptive non-deep-learning framework for underwater image enhancement, successfully overcoming the critical limitations of rigid classification and hard-thresholding methods. By introducing a continuous fuzzy-weighted soft-switching mechanism based on mean chromaticity in the CIE Lab color space, the proposed approach dynamically coordinates three parallel restoration pathways red channel compensation, adaptive white-balance, and gray-world constancy. This architecture effectively mitigates ambiguous, overlapping, and non-uniform color casts without generating artificial boundary artifacts or oversaturation. This quantitative evidence, summarized in Tables 1 and 2 and further supported by the ablation analysis in Tables 3 and 4, indicates that the fuzzy-weighted soft-switching mechanism provides a measurable and consistent improvement over the compared non-deep-learning baselines across both the UIEB and UCCS benchmarks, within the scope of the four no-reference metrics evaluated in this study.

5.1 Limitations

Despite these results, several limitations should be acknowledged. First, the proposed fuzzy weighting scheme is designed around blue, green, and yellow chromatic casts derived from the geometry of the CIE Lab color space; its generalization to less common conditions, such as cyan-dominant casts, mixed artificial-natural illumination, or severe low-light scenes, has not been explicitly validated and remains an open question. Second, the evaluation in this study relies exclusively on no-reference image quality metrics (UCIQE, UIQM, BRISQUE, and PIQE), which capture statistical image characteristics but do not fully represent human visual perception; images that are numerically over-enhanced may still obtain favorable scores under these metrics. Third, the framework's adaptivity is entirely dependent on mean chromaticity statistics computed directly from each input image; scenes with unusual lighting or sensor characteristics that distort these statistics could reduce the reliability of the resulting fuzzy weights. Finally, while Section 4 reports per-image runtime and CPU utilization on a single workstation, demonstrating the pipeline's lightweight, CPU-only design, this study does not include a dedicated memory-footprint or power-consumption evaluation, nor a runtime comparison against deep-learning baselines on embedded hardware, which would be required to fully substantiate real-time embedded deployment claims.

5.2 Future work

Future research will address these limitations along several directions: validating the framework on real-world underwater footage and additional cast conditions beyond the blue-green-yellow taxonomy; complementing the current no-reference metrics with subjective human evaluation and downstream computer vision tasks such as object detection and feature matching; and extending the runtime evaluation reported in Section 4 with memory-footprint, power-consumption, and on-device benchmarking on actual embedded AUV/ROV hardware, including runtime comparisons with deep-learning baselines.

REFERENCES

[1] Zhao, Z.F., Zhou, Z., Lai, Y.T., et al. (2023). Single underwater image enhancement based on adaptive correction of channel differential and fusion. Frontiers in Marine Science, 9: 1058019. https://doi.org/10.3389/fmars.2022.1058019

[2] Huang, S.C., Zhu, Y.J., Huang, X.Y., Xia, X.X., Qian, Z.G. (2024). Programmable adhesion and morphing of protein hydrogels for underwater robots. Nature Communications, 15: 195. https://doi.org/10.1038/s41467-023-44564-6

[3] Zhang, W.H., Li, X.B., Huang, Y.Z., Xu, S.P., Tang, J.W., Hu, H.F. (2025). Underwater image enhancement via frequency and spatial domains fusion. Optics and Lasers in Engineering, 186: 108826. https://doi.org/10.1016/j.optlaseng.2025.108826

[4] Zhang, W.H., Li, X.B., Xu, S.P., et al. (2023). Underwater image restoration via adaptive color correction and contrast enhancement fusion. Remote Sensing, 15(19): 4699. https://doi.org/10.3390/rs15194699

[5] Lin, Y.H., Yu, C.M., Wu, C.Y. (2021). Towards the design and implementation of an image-based navigation system of an autonomous underwater vehicle combining a color recognition technique and a fuzzy logic controller. Sensors, 21(12): 4053. https://doi.org/10.3390/s21124053

[6] Hu, K.J., Pan, Y.T., Jiang, L.W., Lee, S.D., Kao, S.L. (2025). A robust underwater image enhancement algorithm. The Journal of Supercomputing, 81: 244. https://doi.org/10.1007/s11227-024-06719-0

[7] He, K.M., Sun, J., Tang, X.O. (2009). Single image haze removal using dark channel prior. In 2009 IEEE Conference on Computer Vision and Pattern Recognition, Miami, FL, USA, pp. 1956-1963. https://doi.org/10.1109/CVPR.2009.5206515

[8] Hitam, M.S., Awalludin, E.A., Wan Yussof, W.N.J.H., Bachok, Z. (2013). Mixture contrast limited adaptive histogram equalization color models for underwater image enhancement. In 2013 International Conference on Computer Applications Technology (ICCAT), Sousse, Tunisia, pp. 1-5. https://doi.org/10.1109/ICCAT.2013.6522017

[9] Zhao, L.Q., Li, Y.D., Zhong, T. (2025). A generative adversarial network with multiscale and attention mechanisms for underwater image enhancement. Scientific Reports, 15: 2787. https://doi.org/10.1038/s41598-025-86949-1

[10] Ren, T.D., Xu, H.Y., Jiang, G.Y., Yu, M., Zhang, X., Wang, B. (2022). Reinforced swin-convs transformer for simultaneous underwater sensing scene image enhancement and super-resolution. IEEE Transactions on Geoscience and Remote Sensing, 60: 1-16. https://doi.org/10.1109/TGRS.2022.3205061

[11] Ding, X.Y., Chen, X.Y., Sui, Y.X., Wang, Y.F., Zhang, J.X. (2025). Underwater image enhancement using a diffusion model with adversarial learning. Journal of Imaging, 11(7): 212. https://doi.org/10.3390/jimaging11070212

[12] Shi, X.W., Wang, Y.G. (2024). CPDM: Content-preserving diffusion model for underwater image enhancement. Scientific Reports, 14: 31309. https://doi.org/10.1038/s41598-024-82803-y

[13] Varghese, N., Kumar, A., Rajagopalan, A.N. (2023). Self-supervised monocular underwater depth recovery, image restoration, and a real-sea video dataset. In 2023 IEEE/CVF International Conference on Computer Vision (ICCV), Paris, France, pp. 12214-12224. https://doi.org/10.1109/ICCV51070.2023.01125

[14] Peng, L.T., Zhu, C.L., Bian, L.H. (2023). U-shape transformer for underwater image enhancement. IEEE Transactions on Image Processing, 32: 3066-3079. https://doi.org/10.1109/TIP.2023.3276332

[15] Cong, X.F., Zhao, Y., Gui, J., Hou, J.M., Tao, D.C. (2026). A comprehensive survey on underwater image enhancement based on deep learning. IEEE Transactions on Emerging Topics in Computational Intelligence, 10(4): 2783-2801. https://doi.org/10.1109/TETCI.2026.3668671

[16] Peng, Y.T., Cosman, P.C. (2017). Underwater image restoration based on image blurriness and light absorption. IEEE Transactions on Image Processing, 26(4): 1579-1594. https://doi.org/10.1109/TIP.2017.2663846

[17] Song, W., Wang, Y., Huang, D.M., Tjondronegoro, D. (2018). A rapid scene depth estimation model based on underwater light attenuation prior for underwater image restoration. In 19th Pacific-Rim Conference on Multimedia, Hefei, China, pp. 678-688. https://doi.org/10.1007/978-3-030-00776-8_62

[18] Zhang, J.N., Yu, Q., Hou, G.J. (2024). Underwater image restoration via adaptive color correction and dehazing. Applied Optics, 63(10): 2728-2736. https://doi.org/10.1364/AO.514749

[19] Li, X.J., Hou, G.J., Li, K.Q., Pan, Z.K. (2022). Enhancing underwater image via adaptive color and contrast enhancement, and denoising. Engineering Applications of Artificial Intelligence, 111: 104759. https://doi.org/10.1016/j.engappai.2022.104759

[20] Zhang, W.D., Zhuang, P.X., Sun, H.H., Li, G.H., Kwong, S., Li, C.Y. (2022). Underwater image enhancement via minimal color loss and locally adaptive contrast enhancement. IEEE Transactions on Image Processing, 31: 3997-4010. https://doi.org/10.1109/TIP.2022.3177129

[21] Wang, Z.B., Zhou, D.J., Li, Z.C., Yuan, Z.Z., Yang, C. (2024). Underwater image enhancement via adaptive color correction and stationary wavelet detail enhancement. IEEE Access, 12: 11066-11082. https://doi.org/10.1109/ACCESS.2024.3354169

[22] Shi, J.Y., Yu, S.S., Li, H.N., Zhang, X.G., Liu, C.X. (2023). Underwater image enhancement based on adaptive color correction and multi-scale fusion. Multimedia Tools and Applications, 83: 12535-12559. https://doi.org/10.1007/s11042-023-15652-y

[23] Zhang, W.D., Liu, Q.M., Lu, H.M., Wang, J.P., Liang, J. (2025). Underwater image enhancement via wavelet decomposition fusion of advantage contrast. IEEE Transactions on Circuits and Systems for Video Technology, 35(8): 7807-7820. https://doi.org/10.1109/TCSVT.2025.3545595

[24] Zhang, W.D., Wang, M.Z., Zhuang, P.X., Liu, D.H. (2025). Underwater image enhancement via advantage feature weighted fusion. IEEE Transactions on Circuits and Systems for Video Technology, 36(2): 2006-2018. https://doi.org/10.1109/TCSVT.2025.3603059

[25] Yan, J.Q., Hu, H., Wang, Y.J., et al. (2025). Underwater

image enhancement via multiscale disentanglement strategy. Scientific Reports, 15: 6076. https://doi.org/10.1038/s41598-025-89109-7

[26] Veeresh, Thillaigovindan, S.K. (2026). Underwater image enhancement using channel-adaptive frequency-spatial network (CAFS-Net). International Journal of Intelligent Engineering and Systems, 19(3): 472-484. https://doi.org/10.22266/ijies2026.0331.29

[27] Li, C.Y., Guo, C.L., Ren, W.Q., Cong, R.M., Hou, J.H., Kwong, S. (2020). An underwater image enhancement benchmark dataset and beyond. IEEE Transactions on Image Processing, 29: 4376-4389. https://doi.org/10.1109/TIP.2019.2955241

[28] Liu, R.S., Fan, X., Zhu, M., Hou, M.J., Luo, Z.X. (2020). Real-world underwater enhancement: Challenges, benchmarks, and solutions under natural light. IEEE Transactions on Circuits and Systems for Video Technology, 30(12): 4861-4875. https://doi.org/10.1109/TCSVT.2019.2963772

[29] Mittal, A., Moorthy, A.K., Bovik, A.C. (2012). No-reference image quality assessment in the spatial domain. IEEE Transactions on Image Processing, 21(12): 4695-4708. https://doi.org/10.1109/TIP.2012.2214050

[30] Venkatanath, N., Praneeth, D., Sumohana, S.C., Swarup, S.M. (2015). Blind image quality evaluation using perception based features. In 2015 Twenty First National Conference on Communications (NCC), Mumbai, India, pp. 1-6. https://doi.org/10.1109/NCC.2015.7084843

[31] Yang, M., Sowmya, A. (2015). An underwater color image quality evaluation metric. IEEE Transactions on Image Processing, 24(12): 6062-6071. https://doi.org/10.1109/TIP.2015.2491020

[32] Panetta, K., Gao, C., Agaian, S. (2016). Human-visual-system-inspired underwater image quality measures. IEEE Journal of Oceanic Engineering, 41(3): 541-551. https://doi.org/10.1109/JOE.2015.2469915